ISSN: 2688-8645

Aanalytical Modeling of Cutting Tool Wear for Superalloy and Experimental Validation

Lixin Wang, Binglin Li*

College of Mechatronic Engineering, Southwest Petroleum University, Chengdu, Sichuan, 610000, China

*Corresponding author

Abstract

Tool life in superalloy cutting is an important parameter that affects the machining cost and efficiency. In this paper, the wear analysis model of superalloy GH901 cutting tool is established by using minimum energy method. The influence of chip velocity, cutting temperature and positive pressure on the wear are considered. Aiming at three different types of cutting tools, the cutting speed of 40m/min is used to carry out the turning wear experiment on superalloy GH901. The tool life curve is established according to the measurement data of the wear width of the back tool face. The analysis and comparison with the literature model prediction and the experimental results show that the proposed model has a good prediction effect on the wear measurement of superalloy tool. Furthermore, the influence of cutting speed and thermodynamic parameters between tool and workpiece on tool wear are analyzed theoretically.

Keywords

Carbide Tool; Flank Wear; Superalloy; Life Prediction.

1. Introduction

Nickel-based superalloy GH901 is renowned for its high-temperature resistance, superior strength, and excellent toughness, making it widely applicable in fields such as aero engines and gas turbines. However, the machining of superalloys is characterized by significant cutting forces, high cutting temperatures, severe work hardening, and rapid tool wear, which pose critical challenges to achieving efficient and high-quality manufacturing. Numerous scholars have conducted in-depth research on the wear mechanisms involved [1].

Usui et al. [2] developed an analytical model for tool wear based on adhesive wear theory. Jiang Zenghui et al. [3] established a finite element model for carbide tool wear during the machining of high-strength steel based on the Usui model, analyzing the influence of tool geometry on flank wear. Zhang et al. [4] proposed a micro-milling force model that accounts for tool wear and validated its accuracy through cutting experiments on 6061 aluminum alloy. Yan Fugang et al. [5] experimentally investigated the influence of cutting temperature on tool wear under different cutting parameters. Deng Yadi et al. [6] combined theoretical analysis with experimental methods to develop an empirical model correlating cutting time with flank wear based on experimental data from GH901 alloy, thereby establishing a predictive model for tool wear during the machining of GH901 superalloy with carbide tools. Thakur et al. [7] and Bhatt et al. [8] conducted high-speed turning experiments on Inconel 718, concluding that the primary wear mechanisms for carbide tools are abrasive wear and adhesive wear. He Yan et al. [9] proposed an online tool wear monitoring method based on long short-term memory convolutional neural networks, demonstrating high monitoring accuracy. Akhtar et al. [10] found through experiments that adhesive wear is the predominant wear mechanism leading to carbide tool failure during the machining of nickel-based superalloys, occurring across almost all cutting speeds. However, at medium cutting speeds, adhesive wear dominates, while at high cutting speeds, diffusion wear and chemical wear are exacerbated. Huang et al. [11] and Palmai [12] considered flank wear as a result of the combined effects of abrasive wear, adhesive wear, and diffusion wear, establishing flank wear models. However, these studies differ in their perspectives on influencing factors: Huang et al. considered the effects of contact stress and temperature rise on wear rate, while Palmai focused solely on temperature rise. Chang Hao et al. [13] argued that the repeated scratching action of hard particles on the workpiece surface induces fatigue wear in the tool, manifesting as layer-by-layer peeling in the flank contact area. They developed a theoretical model for tool wear based on Hertz contact theory and tribological fatigue, analyzing the influence of cutting parameters on tool wear. Most of the aforementioned models are based on empirical or semi-empirical formulas derived from experimental data. To further investigate the influence of thermo-mechanical coupling parameters between the tool and workpiece on the wear mechanisms of superalloys, it is necessary to establish a theoretical model for predicting tool wear.

2. Analytical Modeling of Tool Wear

The Usui wear model based on the minimum energy principle is expressed as [2]:

$$\frac{dW}{dt} = P\sigma_n V_c e^{-\frac{Q}{T}} \tag{1}$$

In the equation: P and Q are constants; σ_n represents the normal stress on the tool, MPa; V_c denotes the chip velocity, m/min; and T is the cutting temperature of the tool, °C.

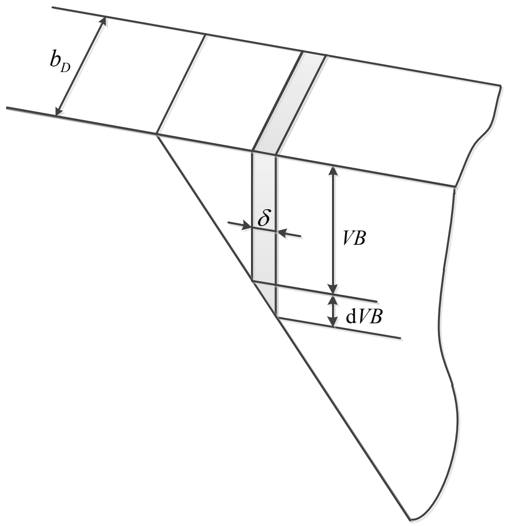

Fig 1. Tool wear micromodel

As shown in Figure 1, the rate of wear change dW per unit time dt is:

$$\mathrm{d}W = b_D(VB + \frac{\mathrm{d}VB}{2})\delta \tag{2}$$

In the equation: b_D represents the width of the cutting tool, in millimeters, mm;VB represents the width of the flank wear on the cutting tool, in millimeters, mm;dVBrepresents the rate of change of the wear width, in millimeters, mm; δ represents the thickness of the newly added wear, in millimeters, mm.

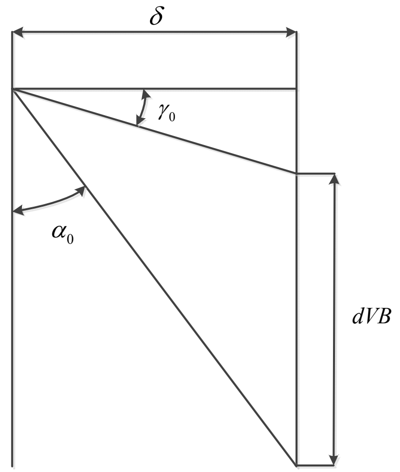

Fig 2. Geometric relationship of wear quantity

As shown in Figure 1:

$$\tan\alpha_0 = \frac{\delta}{\tan\gamma_0\delta + \mathrm{d}VB} \tag{3}$$

According to Equation (3), the wear thickness can be obtained as:

$$\delta = \frac{\tan\alpha_0 \mathrm{d}VB}{1-\tan\alpha_0\tan\gamma_0} \tag{4}$$

$$\mathrm{d}W = b_D(\frac{\tan\alpha_0 \mathrm{d}VB}{1-\tan\alpha_0\tan\gamma_0})(VB+\frac{\mathrm{d}VB}{2}) \tag{5}$$

Since dVB/2 is very small and can be neglected, the above equation simplifies to:

$$\mathrm{d}W = b_D(\frac{\tan\alpha_0 \mathrm{d}VB}{1-\tan\alpha_0\tan\gamma_0})VB \tag{6}$$

The wear rate can be expressed as:

$$\frac{\mathrm{d}W}{\mathrm{d}t} = \frac{\tan\alpha_0}{1-\tan\alpha_0\tan\gamma_0} b_D VB \frac{\mathrm{d}VB}{\mathrm{d}t} \tag{7}$$

Substituting $b_D = \frac{a_p}{\sin\kappa_r}$ into Equation (7), we obtain:

$$\frac{\mathrm{d}W}{\mathrm{d}t} = \frac{\tan\alpha_0}{1-\tan\alpha_0\tan\gamma_0}\frac{a_p}{\sin\kappa_r} VB \frac{\mathrm{d}VB}{\mathrm{d}t} \tag{8}$$

Let $\frac{\tan\alpha_0}{(1-\tan\alpha_0\tan\gamma_0)\sin\kappa_r} = k$,

the above equation simplifies to:

$$\frac{\mathrm{d}W}{\mathrm{d}t} = ka_p VB \frac{\mathrm{d}VB}{\mathrm{d}t} \tag{9}$$

Combining Equation (1) and Equation (9), we obtain:

$$ka_p VB \frac{\mathrm{d}VB}{\mathrm{d}t} = P\sigma_n V_c e^{-\frac{Q}{T}} \tag{10}$$

The above equation can be simplified to:

$$VB\mathrm{d}VB = \frac{P\sigma_n V_c e^{-\frac{Q}{T}}}{ka_p}\mathrm{d}t \tag{11}$$

Integrating both sides, we obtain

$$\frac{VB^2}{2} = \frac{P\sigma_n V_c e^{-\frac{Q}{T}} t}{ka_p} + C_0 \tag{12}$$

Given the initial condition that at t=0, VB=0, it follows that

$$VB = \sqrt{\frac{2P\sigma_n V_c e^{-\frac{Q}{T}} t}{ka_p}} \tag{13}$$

3. Cutting Experiments of Superalloys

3.1. Experimental Conditions

The workpiece material selected for the experiment was a high-temperature alloy GH901 bar with a diameter of 148 mm and a length of 200 mm. Prior to testing, the forged hardening layer on the material surface was removed. The measured hardness of the material was HRC=35.6, and its chemical composition is presented in Table 1.

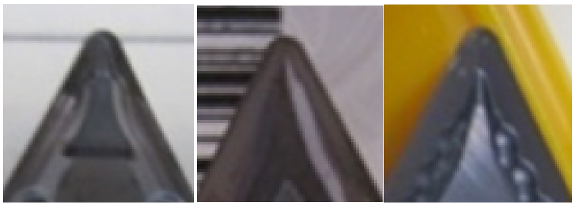

Fig 3. Three types of cutting tools

The machine tool used was a Japanese MAZAK turning-milling compound machining center, with a maximum spindle speed of 4000 r/min. The tool holder employed was a CAPTO tool holder (C6 shank), and the spindle motor power was AC 30KW/22KW. Tool wear was measured using a TRIMOS tool presetter with a 40x magnification, ensuring a measurement precision of 0.01 mm.

Table 1. Chemical composition of GH901 superalloy (wt%)

C	Si	Cr	Ni	Ti	Al
0.031	0.045	12.43	42.2	3.06	0.22
P	B	Cu	Co	Mo	Fe
0.015	0.015	0.003	0.015	6.0	/

The cutting parameters were set as follows: cutting speed V=40 m/min, feed rate of 0.18 mm/rev, and depth of cut of 0.5 mm.

To enhance the accuracy and comparability of the experimental results, the tool wear criterion was defined such that a tool would be considered to have failed when the flank wear width reached VB=0.3mm, or when the surface roughness exceededRa3.2μm. Additionally, the tool life would also be deemed to have ended in the event of severe chip entanglement or burr formation [6]. At the commencement of the experiment, preliminary trial cuts were conducted to establish the time interval for tool edge inspection. Subsequently, throughout the experiment, the tool wear was periodically measured at this predetermined interval using the tool presetter, and the relevant wear data were meticulously recorded.

3.2. Analysis of Experimental Results

Based on the recorded time required to reach specific stages of wear, the experimental data were ultimately compiled, yielding the wear curves for the three types of tools as illustrated in Figure 4.

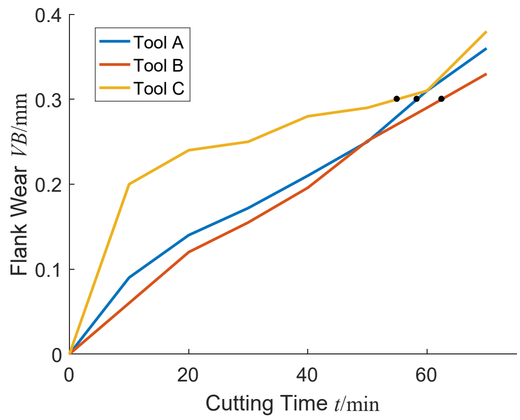

Fig 4. Wear curves of three kinds of tools

Figure 4 displays the wear curves for three types of tools, labeled A, B, and C. The marked points on the graph represent the time points at which each type of tool reached the failure criterion. It can be observed that at a cutting speed of V=40 m/min, the wear curves for all three tools are relatively stable, with wear amount showing a positive correlation with cutting time. However, within the same cutting duration, Tool C exhibited significantly higher wear than the other two types, and its service life was also shorter. In contrast, Tool B demonstrated the best performance among the three, with a slower rate of wear increase and the longest time to reach the failure criterion, amounting to 62 minutes.

4. Experimental Validation and Analysis of the Tool Wear Model

4.1. Comparison of Predicted and Experimental Results for Flank Wear

Based on the normal stress σ_n and cutting temperature T calculated using the DEFORM finite element simulation software, the wear width of the three types of tools can be predicted using Equation (13), where P=0.0000005 and Q=855. The model predictions are compared with the experimental results, as illustrated in Figure 5, 7, and 9:

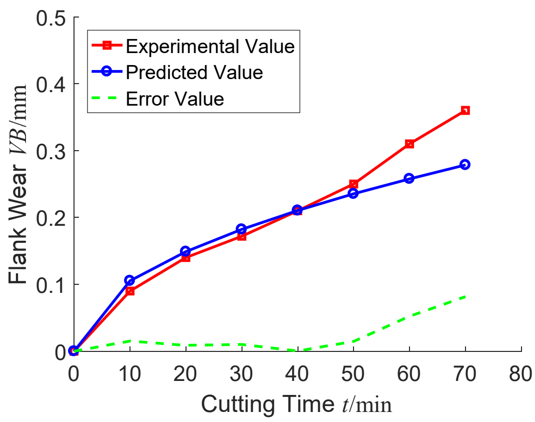

Fig 5. Comparison of the prediction of tool A with experimental results

Fig 6. Final wear state of tool A

The wear value of the flank face of Tool A, as shown in Figure 5, increases significantly during the initial cutting stage. The wear value exceeds 0.1 mm within the time interval of t = 0 to 20 minutes. From t = 20 to 50 minutes, the growth of the wear value is relatively slow. However, during the period from t = 50 to 70 minutes, the wear increases significantly, entering a stage of rapid wear until the tool fails. The predictive model for Tool A demonstrates a relatively accurate prediction effect. Due to the various influences of the actual cutting environment, there is a slight deviation between the predicted results and the experimental data. The minimum absolute error of the wear value VB is 0.002 mm, while the maximum absolute error is 0.068 mm. Figure 6 shows the final wear state of Tool A after cutting at a speed of 40 m/min for 70 minutes, with a flank wear value VB of 0.42 mm and a surface roughness Ra variation below 1.6 μm.

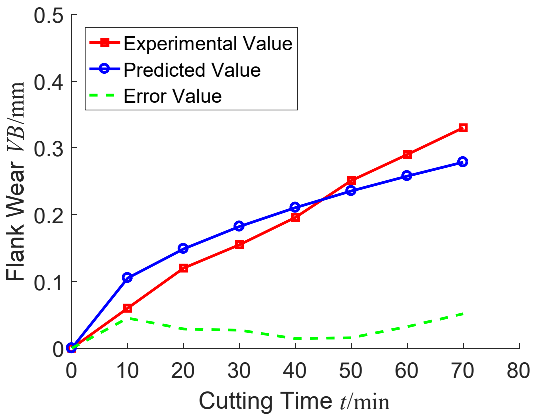

Fig 7. Comparison of the prediction of tool B with experimental results

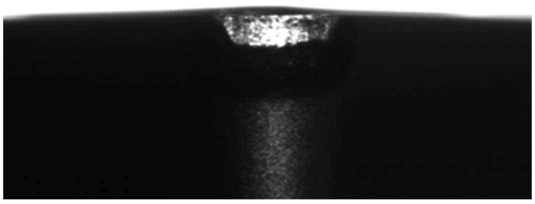

Fig 8. Final wear state of tool B

The wear value of the flank face of Tool B, as shown in Figure 7, increases significantly during the initial cutting stage. The wear value of the tool exceeds 0.1 mm within the time interval of t = 0 to 20 minutes. From t = 20 to 40 minutes, the growth of the wear value is relatively slow. However, during the period from t = 40 to 70 minutes, the wear increases significantly, entering a stage of rapid wear until the tool fails. The predictive model for Tool B demonstrates a relatively accurate prediction effect.

Since the ideal tool model was used during the modeling process, the influence of the tool's geometric factors was not considered. The chips are guided by the chip breaker, allowing them to flow out from the front face in a timely manner, effectively reducing the frictional heat generated by chip contact, which in turn lowers the temperature rise rate of the flank face. The temperature of the flank face is positively correlated with wear, leading to a decrease in wear amount.

Comparing the experimental results, it can be observed that the predicted wear amount is consistently greater than the actual wear amount, which also validates the accuracy of the theoretical analysis. The minimum absolute error of the wear value *VB* is 0.011 mm, while the maximum absolute error is 0.098 mm. Figure 8 shows the final wear state of Tool B after cutting at a speed of 40 m/min for 70 minutes, with a flank wear value *VB* of 0.4 mm and a surface roughness Ra maintained at around 1.6 μm.

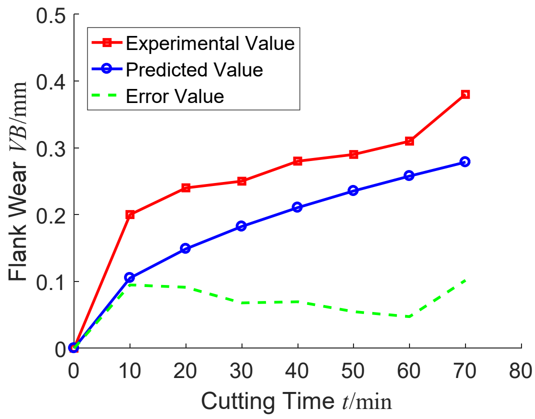

Fig 9. Comparison of the prediction of tool C with experimental results

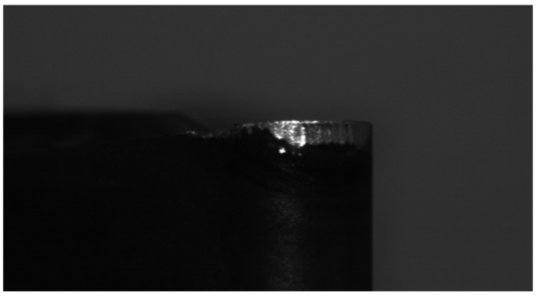

Fig 10. Final wear state of tool C

The wear value of the flank face of Tool C, as shown in Figure 9, increases significantly during the initial cutting stage. The wear value of the tool exceeds 0.1 mm within the time interval of *t* = 0 to 10 minutes. From *t* = 10 to 60 minutes, the growth of the wear value is relatively slow. However, during the period from *t* = 60 to 70 minutes, the wear increases significantly, entering a stage of rapid wear until the tool fails. The predictive model for Tool C demonstrates relatively accurate predictions during the stable wear phase.

Due to the tool surface being coated with a TiAlN layer, the rapid detachment of the coating during the cutting process can lead to a phenomenon of sharp wear increase in the early stages, which affects the accuracy of the predictive model. The maximum absolute error of the wear value VB is 0.129mm. After the tool enters the stable wear phase, the comparison error shows a decreasing trend, with a minimum absolute error of 0.004 mm.

Figure 10 shows the final wear state of Tool C after cutting at a speed of 40 m/min for 70 minutes, with a flank wear value *VB* of 0.357 mm and a surface roughness Ra maintained between 1.0 and 2.0 μm, with Ra consistently decreasing.

ISSN: 2688-8645

4.2. Theoretical Analysis of Tool Wear Prediction Model

According to the tool prediction model proposed in this paper, the effects of cutting speed and thermal parameters between the tool and workpiece on tool wear are analyzed, with the results shown in Figures 11, 12, and 13.

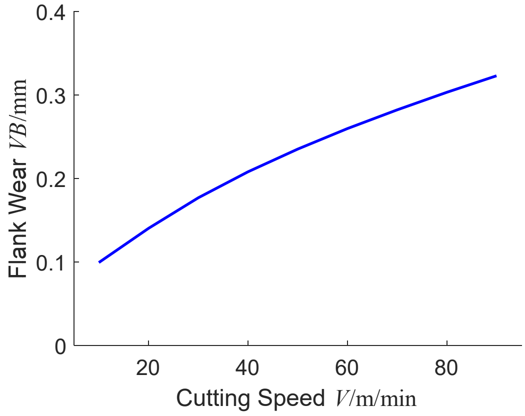

Fig 11. Influence of cutting speed V on the wear of the flank face

Figure 11 shows the effect of cutting speed V on flank wear under the condition of keeping other factors constant. As the cutting speed increases, the wear amount of the flank face shows an upward trend. It can be observed that the cutting speed is approximately proportional to the flank wear amount, indicating that cutting speed has a significant impact on tool wear. Therefore, during the processing of high-temperature alloys, the cutting speed can be appropriately reduced while maintaining the necessary processing efficiency.

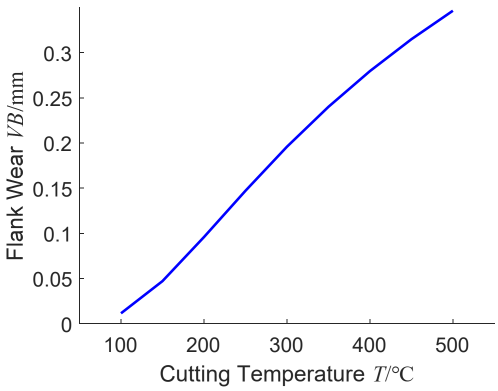

Fig 12. Influence of cutting temperature T on the wear of the flank face

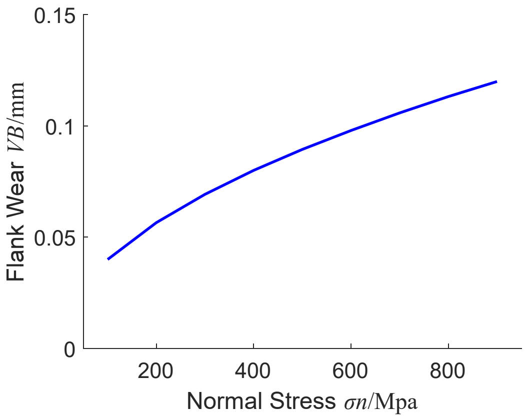

Fig 13. Influence of normal stress σ_n on the wear of the flank face

Figure 12 illustrates the effect of cutting temperature T near the cutting edge on flank wear. As the cutting temperature increases, the wear amount of the flank face shows an upward trend. It can be observed that when the cutting temperature exceeds approximately 150°C, the impact of cutting temperature on flank wear becomes significant.

Figure 13 shows the effect of normal pressure σ_n near the cutting edge on flank wear. As the normal pressure increases, the wear amount of the flank face shows a proportional upward trend. It can be seen that normal pressure has a significant impact on tool wear; therefore, flank wear can be reduced by decreasing the cutting force in the feed direction.

5. Conclusion

A wear analysis model for high-temperature alloy cutting tools was established based on the minimum energy method. The model considers the effects of chip velocity, cutting temperature, and normal pressure on the flank face. The predicted results compared with experimental data indicate that the analysis model has good predictive accuracy for Tool A and Tool B, with errors within the range of 0.1mm. However, the predictive performance for Tool C is relatively poorer compared to Tools A and B, with errors within the range of 0.15mm. These data not only validate the accuracy of the tool wear model but also provide useful references for reducing tool wear during the machining of GH901 high-temperature alloys in actual production processes.

By comparing the comprehensive performance of the three types of tools, it is found that Tool B has a better tool life than Tools A and C, along with good chip-breaking performance, thus exhibiting superior cutting performance.

Additionally, through a single-factor analysis of the proposed model, it can be observed that cutting speed V, cutting temperature T of the flank face, and normal pressure σ_n have a significant impact on the wear amount of the flank face.

References

[1] Zhang Yanan, Niu Shen, Ming Pingmei, et al. Experimental Research on Micro-Pit Array by Jet Electrochemical Machining on GH4169 Nickel-Based Superalloy[J]. Aeronautical Manufacturing Technology, 2024, 67(18): 54-59.

[2] Usui E, Shirakashi T, Kitagawa T. Analytical prediction of cutting tool wear[J]. Wear, 1984, 100(1-3): 129-151.

[3] JIANG Zenghui, SONG Yazhou, JIA Minfei, et al. Research on Simulation of Carbide Tool Wear in Cutting High−Strength Steel Based on The Usui Model[J]. Manufacturing Technology and Machine Tool, 2019, (5): 112-115.

[4] Zhang X, Yu T, Xu P, et al. In-process stochastic tool wear identification and its application to the improved cutting force modeling of micro milling[J]. Mechanical Systems and Signal Processing, 2022, 164: 108233.

[5] Yan Fugang, Lv Yafei, Li Yanguo, Liu Li,Cheng Yaonan, et al. Analysis of High Temperature Wear Process Mechanism of Cemented Carbide Tool[J]. Tool Engineering, 2017, 51(04): 22-27.

[6] Deng Yadi, Li Binglin, Zhang Rui, et al. Experimental Testing and Theoretical Modeling of Tool Wear in Turning GH901 Superalloy[J]. Mechanical Science and Technology for Aerospace Engineering, 2023, 42(12): 2079-2084.

[7] Thakur D G, Ramamoorthy B, Vijayaraghavan L. Study on the machinability characteristics of superalloy Inconel 718 during high speed turning[J]. Materials and Design, 2009, 30(5): 1718-1725.

[8] Bhatt A, Attia H, Vargas R, et al. Wear mechanisms of WC coated and uncoated tools in finish turning of Inconel 718[J]. Tribology International, 2010, 43(5-6): 1113-1121.

[9] He Yan, Ling Junjie, Wang Yulin, et al. In-Process Tool Wear Monitoring Model Based on LSTM-CNN[J]. Chinese Journal of Mechanical Engineering, 2020, 31(16): 1959-1967.

[10] Akhtar W, Sun J, Sun P, et al. Tool wearmechanisms in the machining of Nickel based super-alloys: A review[J]. Frontiers of Mechanical Engineering, 2014, 9: 106-119.

[11] Huang Y, Liang S Y. Modeling of CBN tool flank wear progression in finish hard turning[J]. J. Manuf. Sci. Eng., 2004, 126(1): 98-106.

[12] Pálmai Z. Proposal for a new theoretical model of the cutting tool's flank wear[J]. Wear, 2013, 303(1-2): 437-445.

[13] Chang Hao, Ma Lianjie, Wan Xuewen, et al. Study on Wear Model for Cutting Tools of Machinable Ceramic[J]. Mechanical Science and Technology for Aerospace Engineering, 2020, 39(1): 83-87.